machines

MDPI

Article

Experimental Identification of Milling Process Damping and Its Application in Stability Lobe Diagrams

Cvijetin Mladjenovic [1,*], Katarina Monkova [2,3,*], Aleksandar Zivkovic [1], Milos Knezev [1], Dejan Marinkovic [1] and Vojin Ilic [1]

[1] Faculty of Technical Sciences, University of Novi Sad, 21000 Novi Sad, Serbia; acoz@uns.ac.rs (A.Z.); knezev@uns.ac.rs (M.K.); dejan.marinkovic@uns.ac.rs (D.M.); vojin@uns.ac.rs (V.I.)
[2] Faculty of Manufacturing Technologies with a Seat in Presov, Technical University in Kosice, 080 01 Presov, Slovakia
[3] Faculty of Technology, Tomas Bata University in Zlín, Vavrečkova 5669, 760 01 Zlín, Czech Republic
* Correspondence: mladja@uns.ac.rs (C.M.); katarina.monkova@tuke.sk (K.M.)

Abstract: Self-excited vibrations represent one of the most unfavorable phenomena in the cutting process because they can lead to the accelerated wear or breakage of the tool, a sudden deterioration in the quality of the machined surface, and an increase in noise and energy consumption. To avoid these negative effects, stability diagrams are used when defining the cutting regimes, which, depending on the main spindle speed and the cutting depth, show the border between the stable and unstable machine tool operation states from the aspect of self-excited vibrations. These diagrams, known as "stability lobe diagrams", can be defined using mathematical models (analytical or numerical) or through experimental methods. However, when machining at relatively low main spindle revolutions, process damping occurs, which increases the system stability, i.e., enables a greater cutting depth limit. For the stability diagram to be effectively used for predicting the cutting depth limits at low machining speeds, it is necessary to take the effect of process damping into account. This paper introduces an experimental method for the determination of process damping and its integration into the mathematical framework of the Fourier series method, commonly utilized for the construction of stability lobe diagrams.

Keywords: process damping; self-excited vibrations; frequency analysis; stability lobe diagram

check for updates

Academic Editor: Kai Cheng

Received: 13 December 2024
Revised: 23 January 2025
Accepted: 24 January 2025
Published: 26 January 2025

Citation: Mladjenovic, C.; Monkova, K.; Zivkovic, A.; Knezev, M.; Marinkovic, D.; Ilic, V. Experimental Identification of Milling Process Damping and Its Application in Stability Lobe Diagrams. *Machines* **2025**, *13*, 96. https://doi.org/10.3390/machines13020096

Copyright: © 2025 by the authors. Licensee MDPI, Basel, Switzerland. This article is an open access article distributed under the terms and conditions of the Creative Commons Attribution (CC BY) license (https://creativecommons.org/licenses/by/4.0/).

1. Introduction

Self-excited vibrations, often referred to as chatter, are a critical phenomenon in machining processes, posing significant challenges for achieving stable cutting conditions. These vibrations draw energy directly from the machining process, leading to self-sustaining oscillatory behavior. The consequences of chatter are severe, including reduced surface quality, elevated noise levels, and the accelerated wear of cutting tools and machine components, which collectively impair machining efficiency and productivity [1,2].

To predict and mitigate chatter, stability lobe diagrams (SLDs) are widely employed. These diagrams provide a graphical representation of the boundary between stable and unstable cutting regions based on critical parameters such as spindle speed and depth of cut. SLDs are typically derived using mathematical models, including Fourier series methods [2], tool contact angle methods [3], and advanced numerical simulations of machining processes [4]. However, despite their effectiveness in high-speed machining, these

models face limitations when applied to low-speed operations, where process damping becomes a dominant factor.

Process damping arises from the interaction between the undulated machined surface and the tool flank face (Figure 1a), which generates frictional forces that oppose tool oscillations. This phenomenon is particularly prominent at low spindle speeds, where the increased contact time between the tool and workpiece amplifies the damping effect (Figure 1b) [5]. Process damping plays a critical role in enhancing the dynamic stability of machining systems by increasing the allowable depth of cut in otherwise unstable regions. Consequently, existing mathematical models for predicting the limiting cutting depth require refinement to ensure their applicability under conditions of relatively low cutting speeds [6–10].

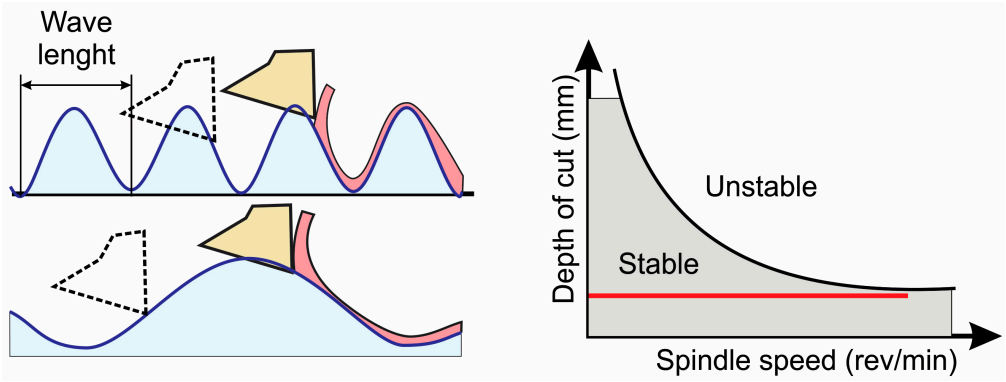


Figure 1. (**a**) The influence of process damping on the SLD; (**b**) contact between the back surface of the tool and the machined surface.

Accurately predicting process damping effects requires the determination of a process damping coefficient, a parameter influenced by material properties, tool geometry, and cutting conditions. Experimental studies [10–12] and advanced modeling techniques have been instrumental in quantifying this coefficient, enabling its integration into stability analyses.

For instance, Budak and Tunc [5] introduced an experimental approach to identify process damping coefficients in turning and milling processes, focusing on materials such as aluminum (Al7075), steel (Ck50), and titanium alloys (Ti6Al4V). Their results demonstrated the significant influence of tool edge geometry on damping behavior.

Gurdal et al. [8] further advanced process damping modeling by introducing an equivalent viscous damping framework. Their work accounted for factors such as tool wear, relief angles, and surface waviness, enabling more accurate predictions of machining stability. Similarly, Orak et al. [13] proposed a novel process damping model specifically designed for milling operations, emphasizing the interplay between cutting parameters and damping effects.

Recent efforts have focused on refining mathematical models to incorporate process damping into stability predictions. Feng and Liu [14] provided a comprehensive review of process damping mechanisms and their integration into machining stability models, highlighting the importance of considering material properties and tool geometry. Kurata et al. [15] investigated chatter stability in turning and milling operations using the in-process identification of process damping coefficients, demonstrating the potential for the real-time adaptation of cutting parameters.

One significant advancement in modeling was proposed by Li et al. [16], who introduced the concept of an anti-vibration relief angle to enhance stability during the milling of thin-walled components. By dividing the tool relief angle into two segments—a smaller

anti-vibration relief angle (α_1) and a standard relief angle (α_2) (Figure 2) [16]—the authors demonstrated an increase in process damping due to prolonged contact between the tool and workpiece. This approach offers practical benefits for machining applications requiring high precision and stability.

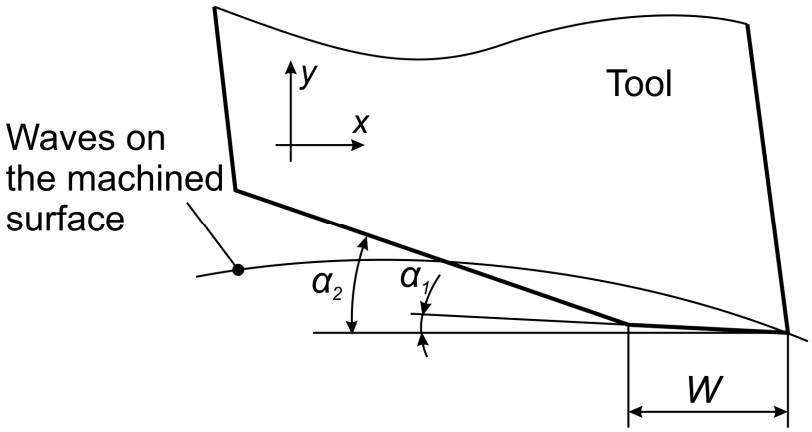


Figure 2. Anti-vibration tool relief angle α_1.

Taylor et al. [17] explored the relationship between tool geometry and process damping, emphasizing the influence of variable helix and pitch angles. Their findings revealed that optimized tool geometries significantly enhance damping effects, reducing the propensity for chatter in milling operations. This work aligns with earlier studies by Yusoff et al. [18], who demonstrated that tools with variable pitch and helix angles can double the process damping effect compared to conventional tools.

Experimental validation remains a cornerstone of process damping research, providing critical data for refining theoretical models. Tyler and Schmitz [10] conducted a comprehensive analysis of the stability of turning and milling processes, incorporating the effects of process damping. This phenomenon was quantified through an experimentally determined damping coefficient, which exhibited a direct dependence on cutting speed. By integrating the identified damping coefficient into Tlusty's [3] mathematical model, the authors developed a stability map. Furthermore, they examined the impact of the tool relief angle and the wear band on the tool flank surface on process damping. Their findings revealed that reducing the relief angle and increasing the wear band enhances process damping, thereby elevating the stability limit at lower spindle speeds.

In separate research [19], the same authors established a database of process damping coefficients for hard-to-machine materials, including steel C18, titanium superalloys (Ti6Al4V), and stainless steels (X5CrNi18). Their work highlighted the role of tool relief angles and wear bands in modulating damping effects, offering insights into optimizing cutting parameters for challenging materials.

Feng and Liu [14] emphasized the importance of combining experimental and analytical approaches, proposing a hybrid methodology that integrates modal analysis with dynamic simulations. This approach enables the more precise identification of damping coefficients, particularly for complex machining scenarios involving multi-axis operations.

Tang and Liu [20] conducted an experimental investigation to evaluate the influence of the tool helix angle and rake angle on the stability of the milling process. Their study demonstrated that an increase in both angles contributes to enhanced process stability, highlighting their critical role in achieving improved machining performance.

By analyzing the previously presented literature, it can be concluded that determining the process damping coefficient represents one of the biggest challenges in the analysis of self-excited vibrations in machining.

This paper presents a new method for implementing an experimentally defined process damping coefficient into the Fourier series method for defining SLDs. To verify the SLDs defined by this improved method, a series of experimental tests were conducted, in which the influence of the machining system modal parameters on the process damping coefficient was analyzed, which can be considered a novelty and a significant contribution of research to the scientific field.

2. Mathematical Modeling of Stability Lobe Diagrams for Machining Systems

The initial phase of the research detailed in this study focuses on the mathematical formulation of the stability lobe diagram (SLD) for the EMCO ConceptMill 450 machining center (Figure 3) utilizing the Fourier series method. The SLD was derived for the milling of a workpiece made of 42CrMo4 steel employing a tool with a diameter of 10 mm.



Figure 3. Machining center EMCO Concept Mill 450.

As previously noted, the stability lobe diagram delineates the boundary between stable and unstable regions of the cutting process as a function of axial cutting depth (b_{lim}) and main spindle speed (Figure 4) [4]. To derive the SLD through a mathematical model, the Altintas–Budak Fourier series model is outlined below [2].

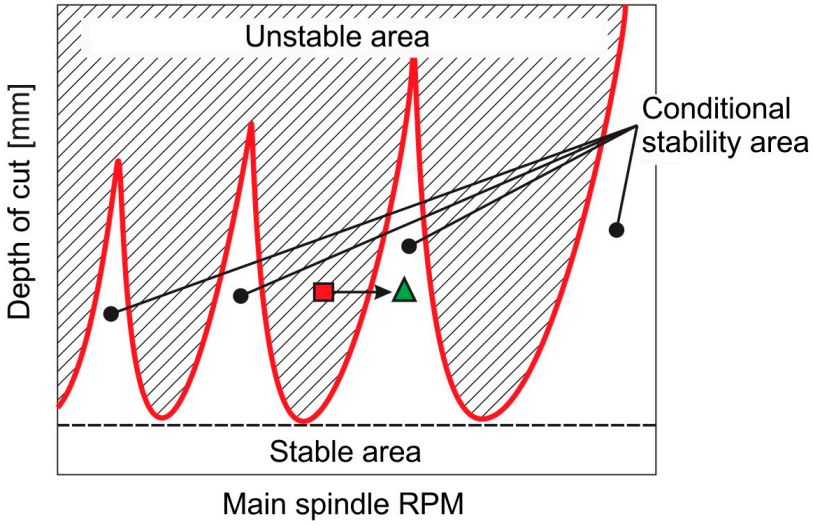


Figure 4. Graphical representation of the stability lobe diagram.

2.1. Definition of SLD Using the Fourier Series Method

To formulate the stability lobe diagram using the Fourier series method, Altintas and Budak conceptualized a milling tool with *Nt* teeth and a helix angle of 0° as a dynamic system with two degrees of freedom (Figure 5). They adopted the following assumptions [2]:

- The oscillatory system is linear.
- The direction of the variable component of the cutting force depends on the tool teeth's current position during the cut.
- The variable component of the cutting force is influenced by oscillations along the X and Y axes of the machining system.
- The magnitude of the variable component of the cutting force varies proportionally and simultaneously with changes in the chip cross-section.
- The system is modeled as a time-variant variable, analyzing stability for each position of the tool during the cut (from ϕ_{st} to ϕ_{ex}).

The axial cutting depth and the main spindle speeds with this model are determined from the following expression:

$$b_{lim} = \frac{2\pi\Lambda_R}{N_t K_t}\left(1+\kappa^2\right) \quad (1)$$

$$n = \frac{60}{NT} \quad (2)$$

where:

Λ_R and Λ_I - the real and imaginary part of the complex quadratic function, which is defined based on the FRF of the observed system, where: $\kappa^2 = \frac{\Lambda_I}{\Lambda_R}$;

$T = \frac{\varepsilon + 2R\pi}{\omega_c}$ - the period between two consecutive tool passes, where R = 0, 1, 2, 3, . . ., and represents the number of "waves" on the SLD;

ω_c - angular velocity of self-excited vibrations;

$\varepsilon = \pi - 2\psi$ - the phase difference between the waves on the machined surface, which are formed by two consecutive tool teeth, where : $\psi = \tan^{-1}\kappa$;

K_t - specific cutting resistance in the tangent direction;

N_t - number of tool teeth.

Self-excited vibrations in cutting arise when the excitation frequency—such as forced vibrations, variations in cutting force intensity due to the regenerative effect, or other external excitations—aligns with the natural frequency of a critical element within the machining system. For robust workpieces, the critical element is commonly the tool–tool holder–main spindle assembly, whereas, for thin-walled workpieces, the workpiece itself becomes the critical element. Considering this, when analyzing self-excited vibrations, or when defining the machining system's stability lobe diagram (SLD), it is essential to understand the modal parameters of the characteristic elements of the machine tool, which are typically determined through experimental modal analysis.

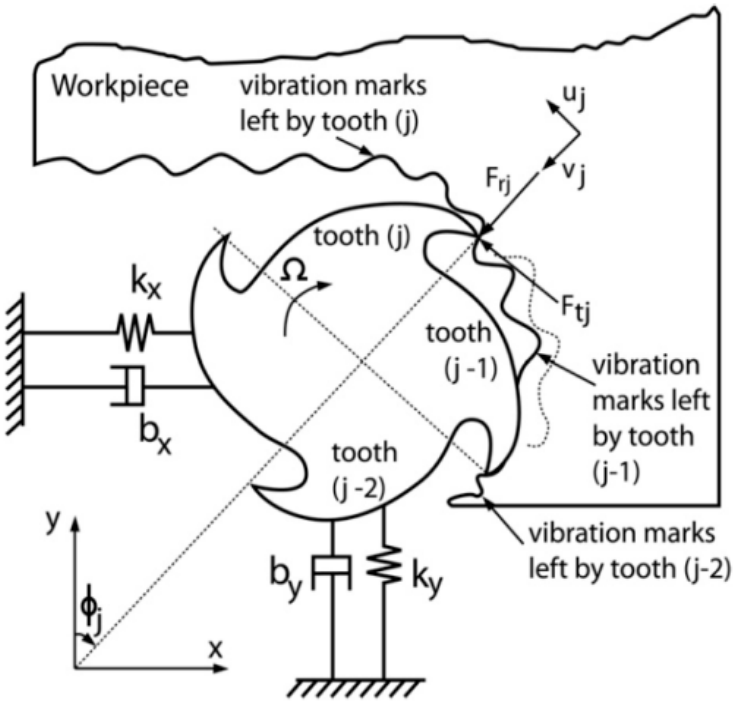


Figure 5. A dynamic milling model with two degrees of freedom.

2.2. Definition of Machining System Modal Parameters

Experimental modal analysis using impulse excitation force is the most straightforward method for determining the frequency response function, and it is frequently utilized to identify the modal parameters of machining systems (Figure 6) [4].

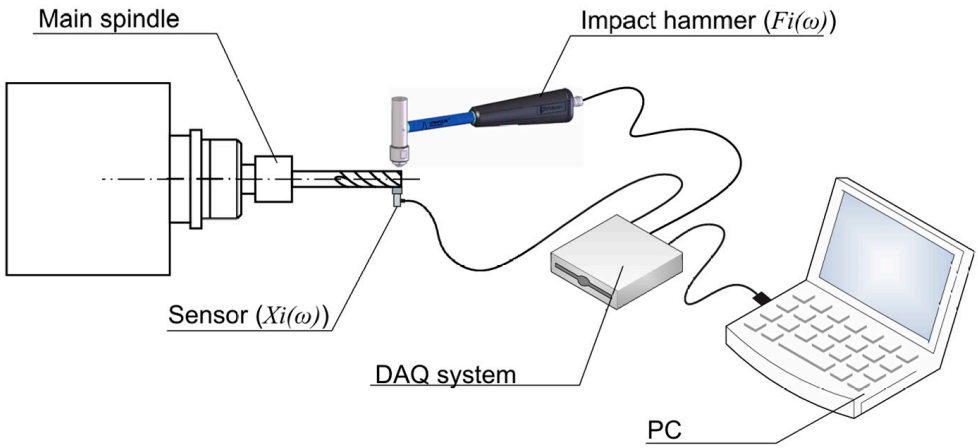


Figure 6. Testing with impulse excitation to determine the frequency response of the system.

By applying impulse excitation, the system is excited by a wide range of different frequencies in just one test. In contrast, the system's response is most often monitored using an acceleration sensor. When the recorded data are transformed into the frequency domain using the fast Fourier transform, the frequency response function between the point where the system response was measured (i) and the point where the excitation force (j) was applied is obtained, which can be displayed as follows.

$$FRF_{ij}(\omega) = \frac{X_i(\omega)}{F_j(\omega)} \tag{3}$$

Also, it should be noted that, in most cases, it is necessary to obtain displacement X as a response of the system. However, if the measurement is performed by acceleration sensors, the previous equation has the following form.

$$\mathrm{FRF}(\omega) = \frac{\ddot{x}}{F(\omega)} = \frac{A(\omega)}{F(\omega)} \tag{4}$$

Converting acceleration into displacement can be achieved by dividing the signal collected by the accelerometer by $(i\omega)^2$, i.e., by $-\omega^2$.

The frequency response function of the system, obtained in the previously described way, is complex, and it consists of a real G and an imaginary H part.

$$\mathrm{FRF}(\omega) = \mathrm{G} + \mathrm{iH} \tag{5}$$

Figure 7 illustrates the real and imaginary components of the frequency response function [4].

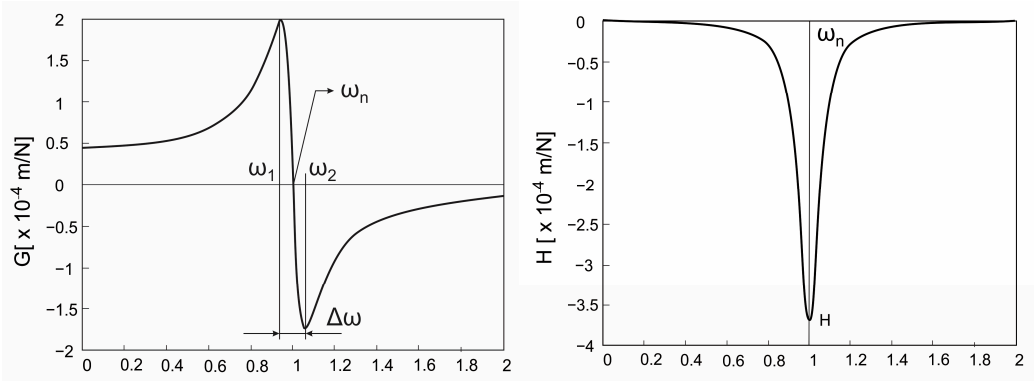


Figure 7. Illustration of the real (**a**) and imaginary (**b**) part of the frequency response function.

The experimentally defined frequency response function, i.e., its real and imaginary parts, are used to calculate the modal parameters of the system [21]:

$\zeta = \frac{\omega_2 - \omega_1}{2\omega_n}$ - dimensionless damping coefficient;

$k = \frac{-1}{2\zeta H}$ - modal stiffness, where H is the minimum of the imaginary part of the FRF for the period between two consecutive tool passes;

$m = \frac{k}{\omega_n^2}$ - modal mass.

Also, if the modal parameters of the system are known, the real and imaginary parts of its frequency response function are calculated using the following expressions:

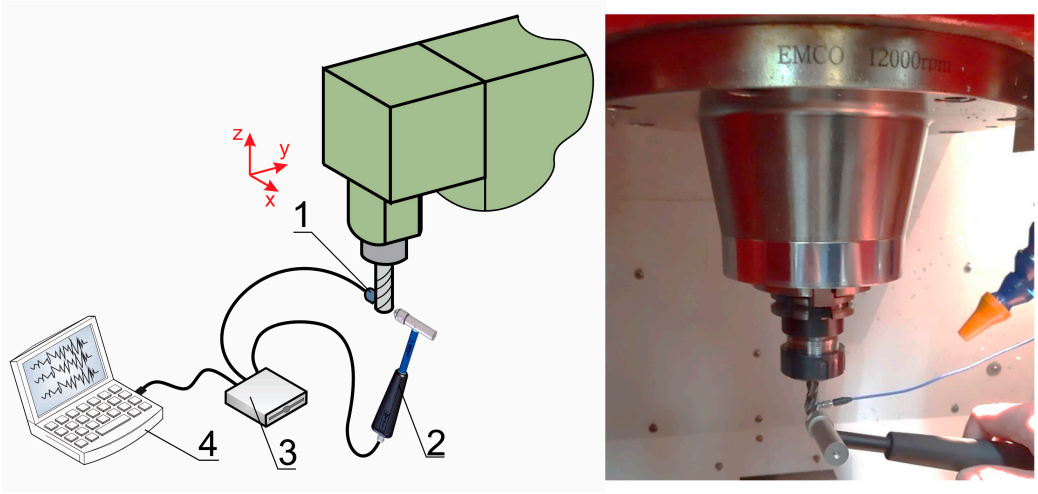
$$\mathrm{Re}\left(\frac{X}{F}\right) = \frac{1}{k}\left(\frac{1 - r^2}{(1-r)^2 + (2\zeta r)^2}\right) \tag{6}$$

$$\mathrm{Im}\left(\frac{X}{F}\right) = \frac{1}{k}\left(\frac{-2\zeta r}{(1-r)^2 + (2\zeta r)^2}\right) \tag{7}$$

where: $r = \frac{\omega}{\omega_n}$.

To determine the modal parameters of the observed processing system, i.e., natural frequency, modal stiffness, and damping coefficient, it is necessary to experimentally

define the system frequency response function. Figure 8a shows the experiment setup for determining the frequency response function of the EMCO ConceptMill 450 machining center, consisting of an acceleration sensor (1), which measures the oscillation of the tooltip, and an excitation hammer (2), which excites the machine structure. The exciting hammer and the acceleration sensor are connected to the A/D card (3), which sends the collected data directly to the computer (4). Figure 8b shows the procedure of experimental modal analysis in the machining center Y-axis direction.



(**a**) (**b**)

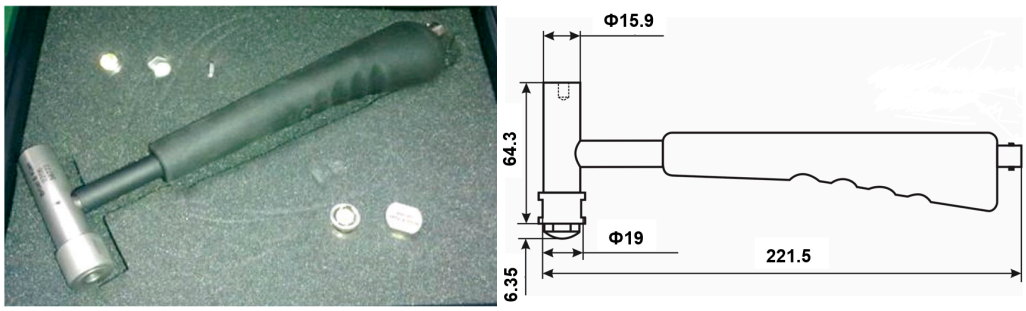
Figure 8. (**a**) The experiment setup. (**b**) The determination of the machining center FRF using the experimental modal analysis procedure.

The excitation of the observed system is achieved using an excitation hammer, the characteristics of which are given in Table 1, and the appearance and dimensions in Figure 9.

Table 1. Characteristics of the excitation hammer.

Manufacturer:	Bruel & Kjaer
Type/Serial No.:	8206/56777
Reference sensitivity at 21.9 °C:	23.28 mV/N
Force measuring range (at ±5 V):	220 N
Operating temperature range:	−73 ÷ +60 °C
Maximum excitation force:	4448 N
Effective seismic mass:	100 g
Additional seismic mass:	40 g
Tip Material:	Aluminum Plastic Rubber

As the FRF of the observed system changes with the change in any element of the system, it should be noted that a tool holder with an effective length of 45 mm is clamped in the machining center's main spindle. The cutting tool that is clamped in the tool holder is a coated carbide endmill with a 10 mm diameter, four cutting edges, and a free length of 35 mm.



(**a**) (**b**)

Figure 9. Exciting hammer: (**a**) appearance; (**b**) basic dimensional characteristics.

Signal acquisition is performed using instrumentation consisting of an acceleration sensor and an analog/digital (A/D) card. The uniaxial acceleration sensor PCB 352C33 (Figure 10a) with a sensitivity of 98.7 mV/g is placed on the top of the tool using special wax so that its measuring axis is in the direction of the excitation force, i.e., in the direction of the X or Y axis of the machine. Signal recording is enabled by A/D card National Instruments USB-4432, (Figure 10b) with five analog inputs, voltage range ±5 V, and maximum signal selection (sampling) speed per channel 104.6 kS/s.



(**a**) (**b**)

Figure 10. Equipment used for experimental modal analysis: (**a**) acceleration sensor PCB 352C33 (**b**) A/D card National Instruments USB-4432.

The signal acquired from the acceleration sensor and the hammer signal are transmitted to a PC via the A/D card, where they are recorded in tabular form using the LabVIEW software system (LabVIEW 2021 SP1). An algorithm is then developed within the MATLAB environment (MATLAB 2024b), facilitating the application of a fast Fourier transform (FFT) to the obtained signals, thereby enabling the determination of the frequency response function of the observed system. The frequency response function of the system is displayed in the form of real and imaginary parts. Figure 11 shows the appearance of the real and imaginary parts of the FRF system measured in the direction of the X axis and, in Figure 12, measured in the direction of the Y axis.

To define the SLD, data on the workpiece material and the machining process are also needed in addition to the modal parameters, which are determined from the shown real and imaginary parts of the FRF. These data and the calculated modal parameters are shown in Table 2.

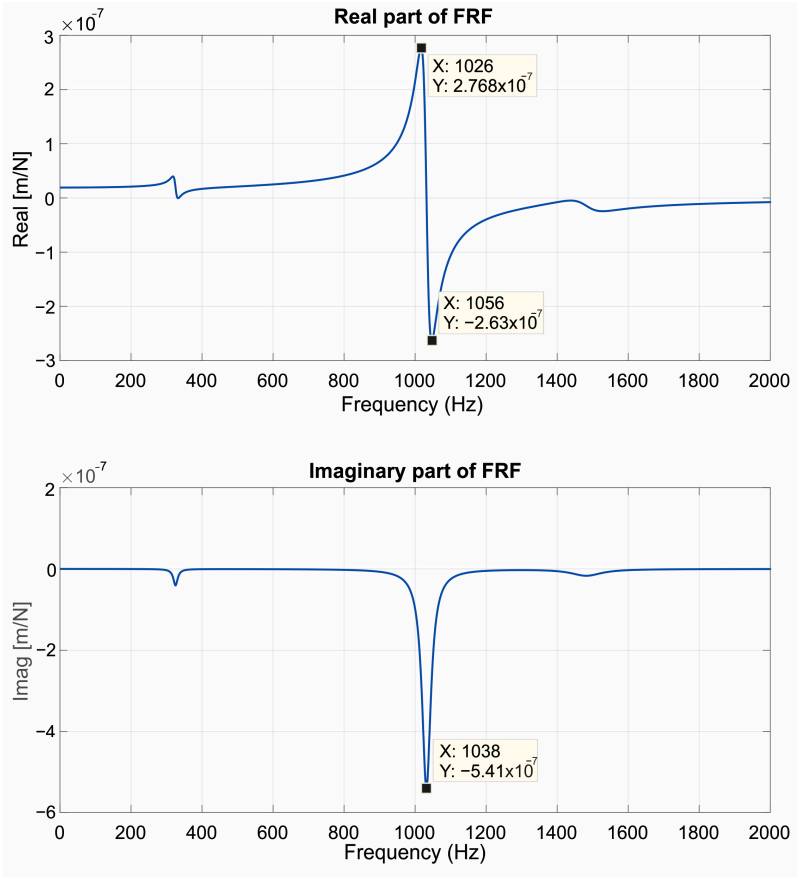


Figure 11. Real and imaginary part of the FRF of the analyzed machining center in the X axis direction.

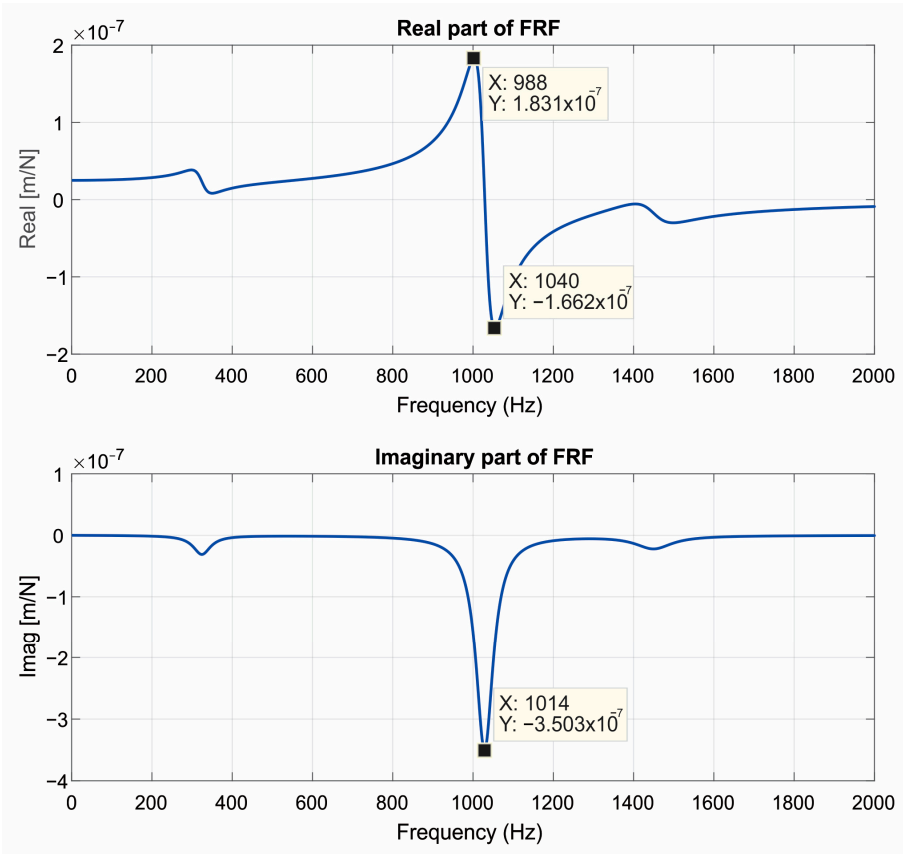


Figure 12. Real and imaginary part of the FRF of the analyzed machining center in the Y axis direction.

Table 2. Parameters needed to define the SLD.

Natural frequency in the X-axis direction:	$\omega_{nx} = 1038$ Hz
Damping coefficient in the X-axis direction:	$\zeta_x = 0.016$
Modal stiffness in the X-axis direction:	$k_x = 1.04 \times 10^8$ N/m
Natural frequency in the Y-axis direction:	$\omega_{ny} = 1014$ Hz
Damping coefficient in the Y-axis direction:	$\zeta_y = 0.038$
Modal stiffness in the Y-axis direction:	$k_y = 6.63 \times 10^7$ N/m
Tool entry angle:	$\phi_{st} = 0^\circ$
Tool exit angle:	$\phi_{ex} = 180^\circ$
Cutting tool characteristics (diameter and number of teeth):	$d = 10$ mm; $N_t = 4$

For the observed frequency range of self-excited vibrations, using Equations (1) and (2) and the data presented in Table 2, the stability limit of the EMCO ConceptMill 450 machining center was defined and visualized on the stability lobe diagram (SLD) (Figure 13).

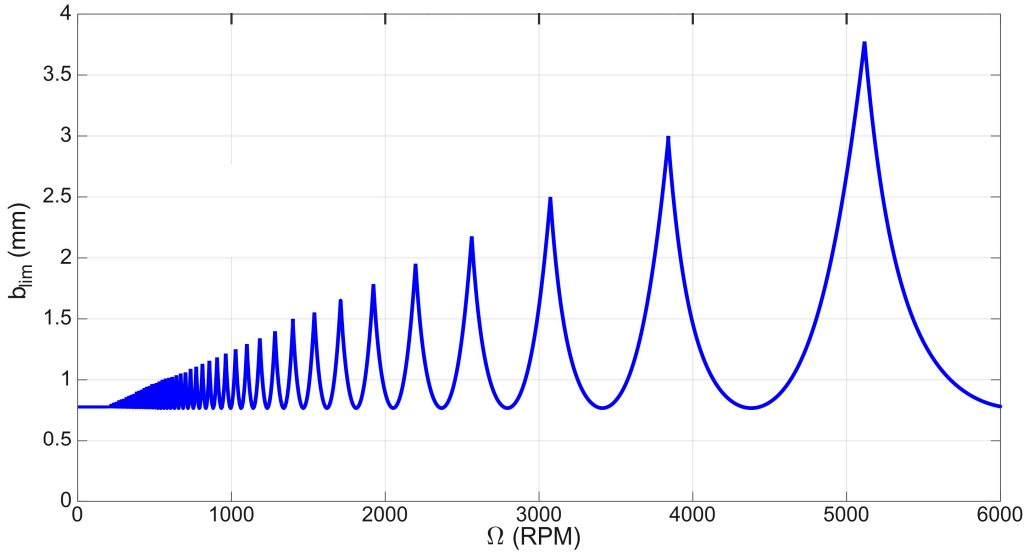


Figure 13. SLD of the EMCO ConceptMill 450 machining center defined by the Fourier series method.

3. Self-Excited Vibration Detection Methods in Experimental Conditions

When analyzing self-excited vibrations in machining, it is necessary to know the natural frequencies of the machine tool's characteristic elements. Namely, according to the theory, self-excited vibrations in cutting processes occur when the excitation frequency—such as forced vibrations, variations in cutting force intensity due to the regenerative effect, or other external excitations—matches the natural frequency of the critical element within the machining system. For robust workpieces, the critical element is typically the assembly of tool, tool holder, and main spindle. In contrast, when machining thin-walled workpieces, the critical element becomes the workpiece itself.

One of the methods for detecting self-excited vibrations is based on conducting a series of experiments while varying the axial depth of the cut and the machine tool's main spindle speed. For one observed main spindle speed, with each pass, the cutting depth is increased by the corresponding increment, while the tool oscillation amplitude is recorded by adequate acquisition equipment. The cutting depth at which self-excited vibrations

occur is considered the limit depth for the observed spindle speed, and the procedure is repeated for each subsequent main spindle number of revolutions. The vibration signal, recorded in the previously described way, is stored in the time domain, and as such does not provide much information about the vibration characteristics. For this reason, it is necessary to transform the recorded vibration signal into the frequency domain using a fast Fourier transformation (Figure 14).

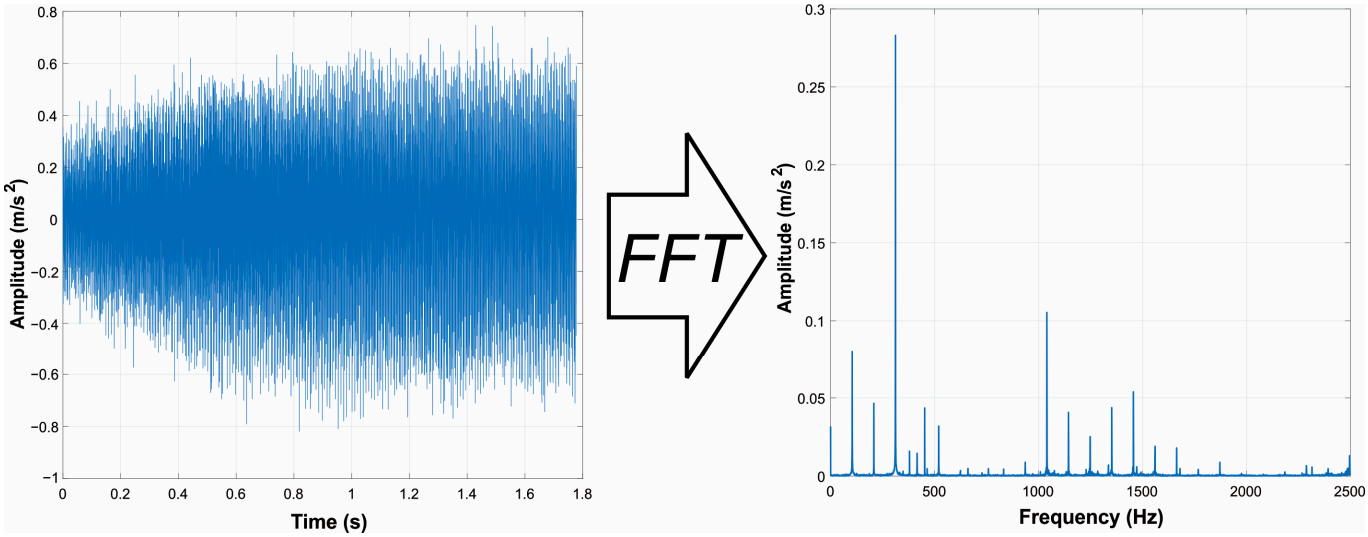


Figure 14. Transformation of vibration signals from time to frequency domain.

In the frequency domain, one can clearly see vibration frequencies that correspond to characteristic phenomena during the cutting process, the most influential of which is the rotation of the main spindle and its harmonics (Figure 15).

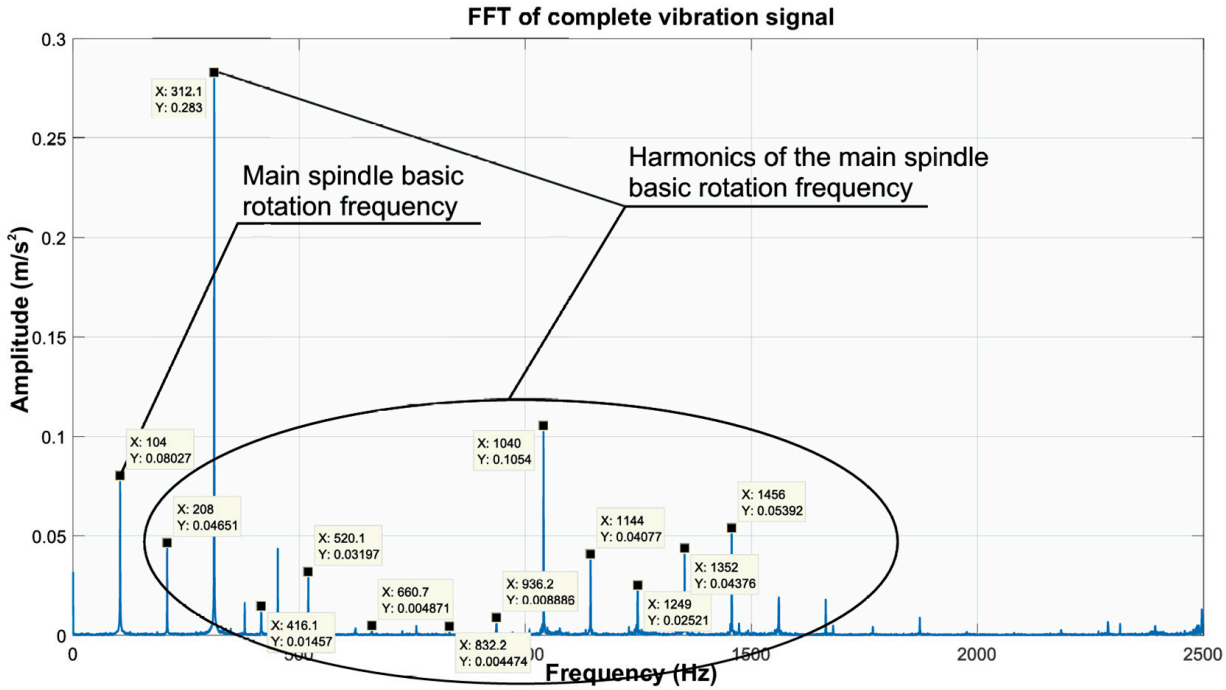


Figure 15. The basic main spindle rotation frequency during cutting and its harmonics.

When the cutting depth exceeds the critical value, a frequency near the natural frequency of the critical element (e.g., the tool–tool holder–main spindle assembly) becomes

apparent in the vibration signal's frequency characteristics. This cutting depth is thereby identified as the limiting value for a specific spindle speed (Figure 16). This testing method can be used to verify mathematically defined SLDs by incrementally increasing the cutting depth from some initial value until self-excited vibrations appear for each significant spindle speed. For each tool pass, a vibration signal is acquired and analyzed to decide whether the self-excited vibrations occur or not.

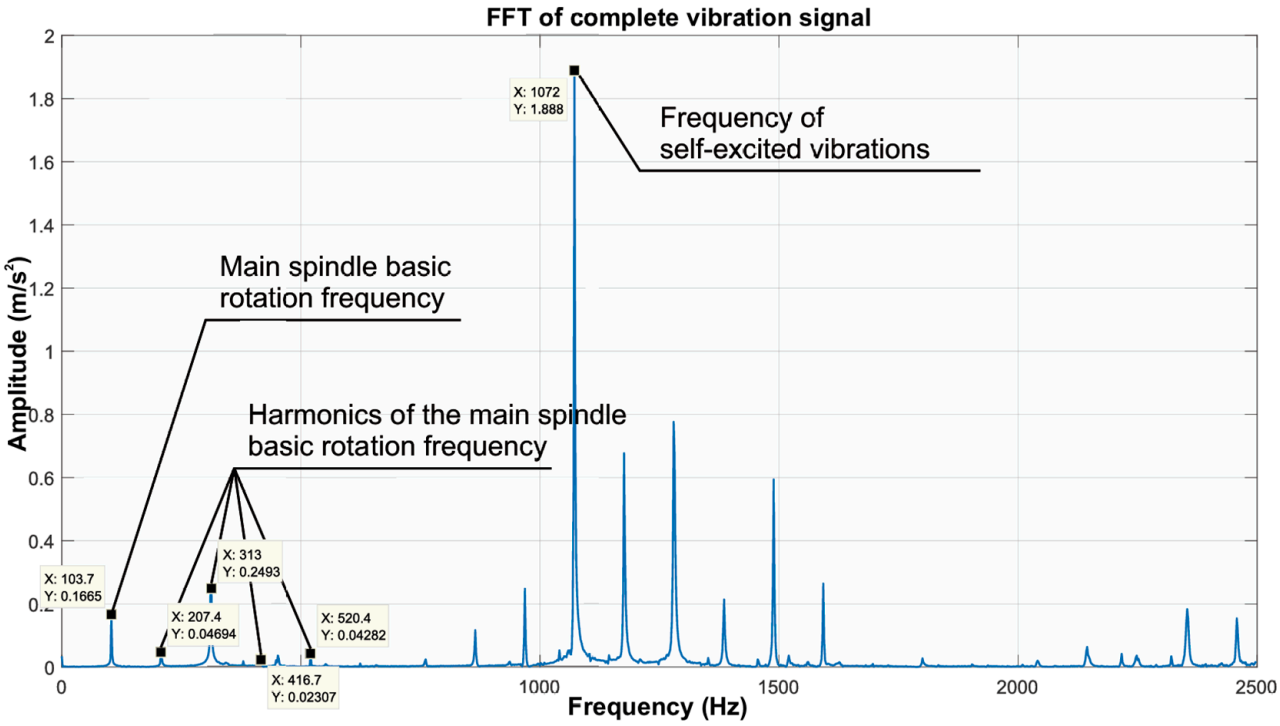


Figure 16. The occurrence of the self-excited vibration frequency in the frequency domain.

4. Experimental Determination of Process Damping in Milling

Defining the SLDs using the Fourier series method gives good results in predicting the limiting depth of cut for a specific machining system. However, at relatively low main spindle speeds, the accuracy of this method decreases due to the influence of the so-called process damping [5,7–10,12,16].

As already mentioned, process damping is a phenomenon where the waviness of the machined surface due to the friction between the machined surface and the tool's flank surface. This damping directly depends on the process damping coefficient, which is most often determined experimentally.

To experimentally determine the process damping coefficient, 36 experiments were conducted in which the cutting depth was varied by an increment of 0.2 mm for seven different spindle speeds. In other words, from the initial depth of cut (0.4 mm) for one spindle speed, the depth of cut was increased by 0.2 mm with each tool pass until the occurrence of self-excited vibrations. After that, the experiment was repeated for the next spindle speed. The influence of the change in the workpiece's dynamic parameters due to the change in its dimensions was neglected because a massive robust workpiece was used, and the dynamic characteristics of this type of workpiece changed minimally during the experiment. The selected spindle speeds fall within the recommended cutting speed range for machining 42CrMo4 steel [22]. The experiments were performed at the EMCO ConceptMill 450 machining center, utilizing a 10 mm diameter high-speed steel tool coated with titanium–aluminum–nitride (TiAlN). The feed per tooth was maintained at a constant

value of 0.02 mm/tooth (Figure 17). The cutting conditions for all 36 experiments are presented in Table 3.

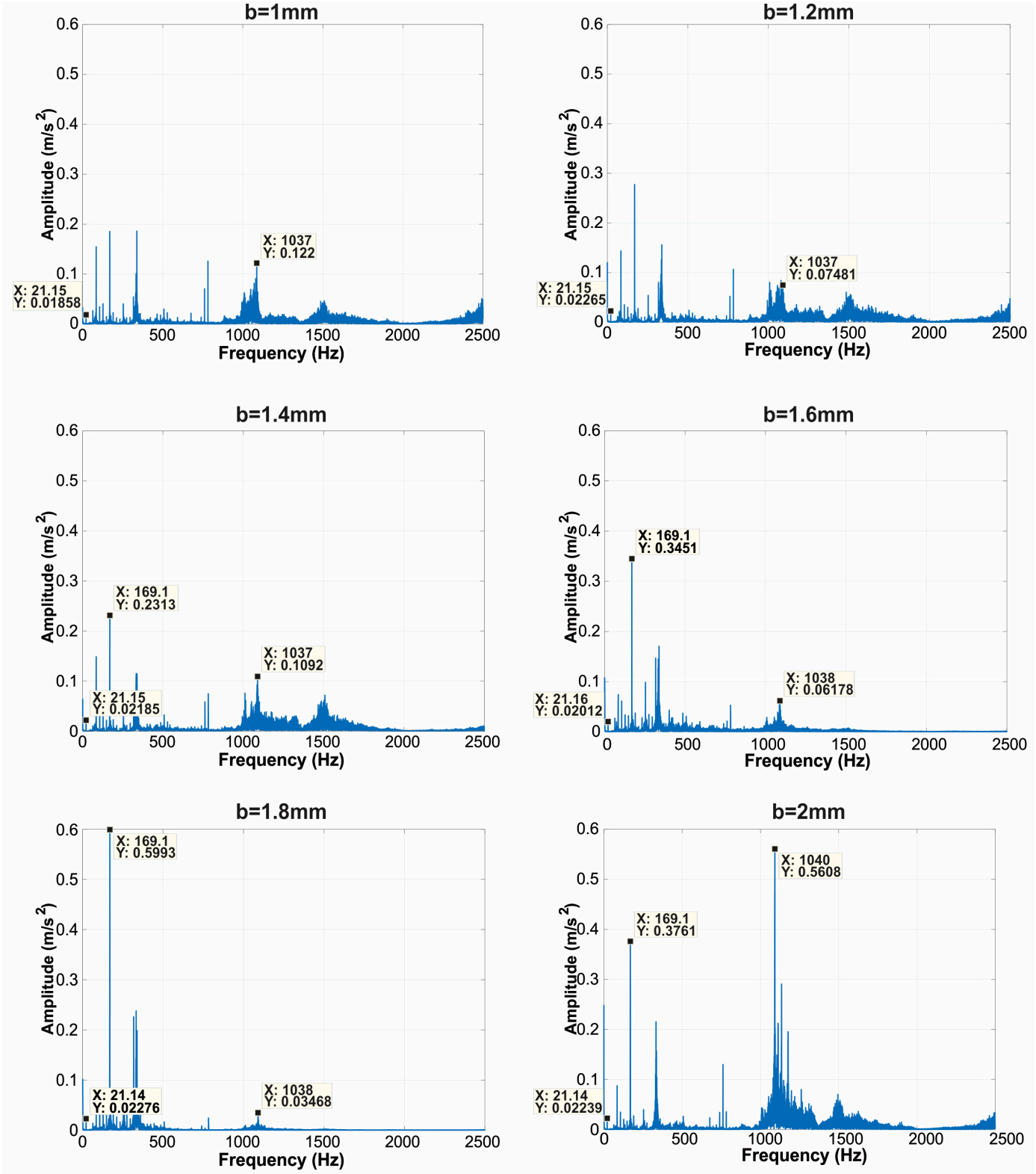


Figure 17. Results of the Fourier transform of the vibration signal for the lowest spindle speed tested.

Table 3. Parameters needed to define the SLD.

No.	Cutting Speed (m/min)	Spindle Speed (rev/min)	Feed (mm/min)	Cutting Depth (mm)
1.	40	1270	101.6	0.4
2.				0.6
3.				0.8
4.				1.0
5.				1.2
6.				1.4
7.				1.6
8.				1.8
9.				2
10.	50	1585	126.8	0.4
11.				0.6
12.				0.8
13.				1.0
14.				1.2
15.				1.4
16.	60	1910	152.8	0.4
17.				0.6
18.				0.8
19.				1.0
20.				1.2
21.	70	2225	178	0.4
22.				0.6
23.				0.8
24.				1.0
25.				1.2
26.	80	2550	204	0.4
27.				0.6
28.				0.8
29.				1.0
30.	90	2865	229.2	0.4
31.				0.6
32.				0.8
33.				1.0
34.	100	3200	256	0.4
35.				0.6
36.				0.8

The detection of self-excited vibrations was performed through the frequency analysis of vibration signals, as described earlier in this paper, with partial results for the lowest spindle speed shown in Figure 17.

Figure 15 clearly shows that, for cutting depths up to 1.8 mm, the vibration amplitude at a frequency close to the main spindle assembly natural frequency (≈1038 Hz) is relatively unnoticeable and small, which leads to the conclusion that self-excited vibrations did not occur in these cases. In the final case, a significant increase in the frequency amplitude of self-excited vibrations is observed when the cutting depth reaches 2 mm. This observation suggests that the limiting depth of cut for a spindle speed of 1270 rpm is 2 mm.

Table 4 presents the limit cutting depths for all observed spindle speeds. It also includes the cutting depths obtained from the SLD defined using the Fourier series method (Figure 10).

Table 4. Comparison of limiting depths of cut defined by experimental tests and by SLD.

No.	Spindle Speed (rev/min)	b_{lim} (mm)		Percentage Deviation (%)
		Experiment	*SLD*	
1.	1270	2	1.1	45
2.	1585	1.4	0.89	36
3.	1900	1.2	1.38	−15
4.	2225	1.0	1.49	−24
5.	2550	1.0	1.36	−36
6.	2865	1.0	0.85	15
7.	3200	0.8	1.215	−52

The analysis of Table 4 reveals a significant disparity between the limit cutting depths predicted by the Fourier series method and those determined through experimental testing. This deviation is attributed to process damping, which becomes significant at lower cutting speeds. Therefore, it is necessary to determine the process damping coefficient and use it to adjust the algorithm for predicting stability limits with the Fourier series method.

Establishing the growth behavior of the experimentally determined limit cutting depths is necessary to determine the cutting process's damping coefficient. Since the increase in limit depth as the spindle speed decreases follows an exponential trend, process damping is determined by fitting an exponential curve to the experimentally obtained limit depths at lower spindle speeds (Equation (8), Figure 18).

$$b_{lim} = 6.9389e^{(-1.13495 \cdot 10^{-3}\Omega)} + 0.69664e^{(-1.4522 \cdot 10^{-6}\Omega)} \quad (8)$$

By analyzing Figure 18, it can be concluded that the change in the critical cutting depth due to the damping of the cutting process follows an exponential trend. With this in mind, the idea emerged to determine the process damping coefficient in correlation with the method of determining the damping coefficient in highly damped mechanical systems.

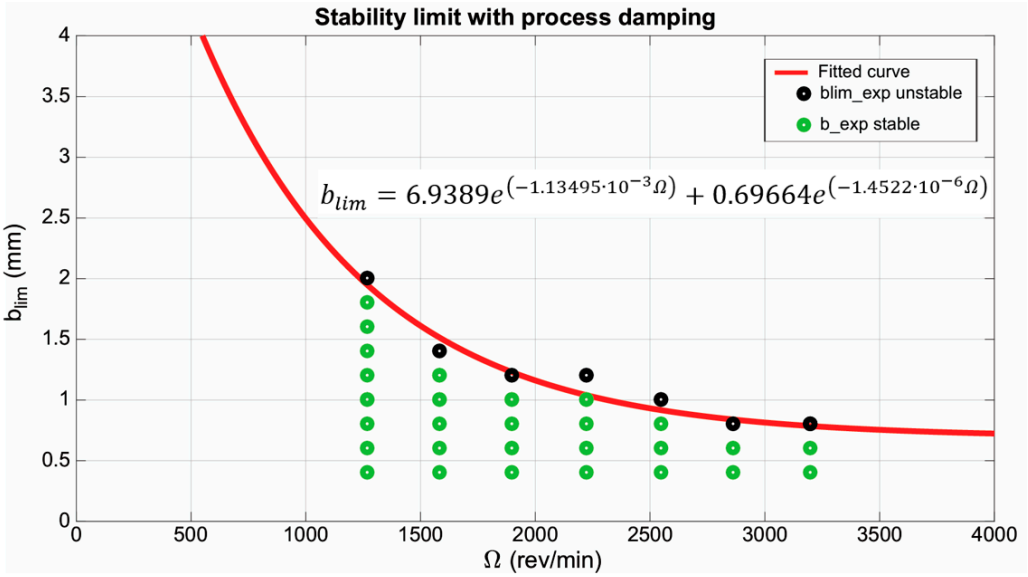


Figure 18. Exponential curve for determining the cutting process damping.

In highly damped mechanical systems, the damping coefficient is determined from the equation of motion [23] as follows:

$$m\ddot{x} + c\dot{x} + kx = 0 \quad (9)$$

where:

k—the modal stiffness of the oscillating system,

$m = \frac{k}{\omega_n{}^2}$—the modal mass of the oscillating system, and

c—the viscous damping of the oscillating system.

It is possible to solve this equation using the equation $x = e^{st}$, where t is time and s is an unknown constant. By differentiating this equation and converting it into Equation (9), an algebraic solution is obtained, which represents a significant simplification of the problem.

$$\left(ms^2 + cs + k\right)e^{st} = 0 \tag{10}$$

The solution to this quadratic equation is as follows.

$$s_{1,2} = -\frac{c}{2m} \pm \sqrt{\left(\frac{c}{2m}\right)^2 - \frac{k}{m}} \tag{11}$$

Thus, $e^{s_1 t}$ and $e^{s_2 t}$ become the solution of Equation (9). The general solution of this equation is the following:

$$x = C_1 e^{s_1 t} + C_2 e^{s_2 t} \tag{12}$$

$$x = C_1 e^{(-\frac{c}{2m} + q)t} + C_2 e^{(-\frac{c}{2m} - q)t} \tag{13}$$

where C_1 and C_2 are arbitrary constants and $q = \sqrt{\left(\frac{c}{2m}\right)^2 - \frac{k}{m}}$.

In discussing the physical significance of this equation, two distinct cases must be considered depending on whether the expressions for s in Equation (10) are real or complex. When $\left(\frac{c}{2m}\right)^2 > \frac{k}{m}$, the term under the radical is positive, resulting in two real values for s. Moreover, both values are negative, as the square root term is smaller than $\frac{c}{2m}$. Thus, Equation (13) represents a solution comprising the sum of two decaying exponential functions, as illustrated in Figure 19 [23].

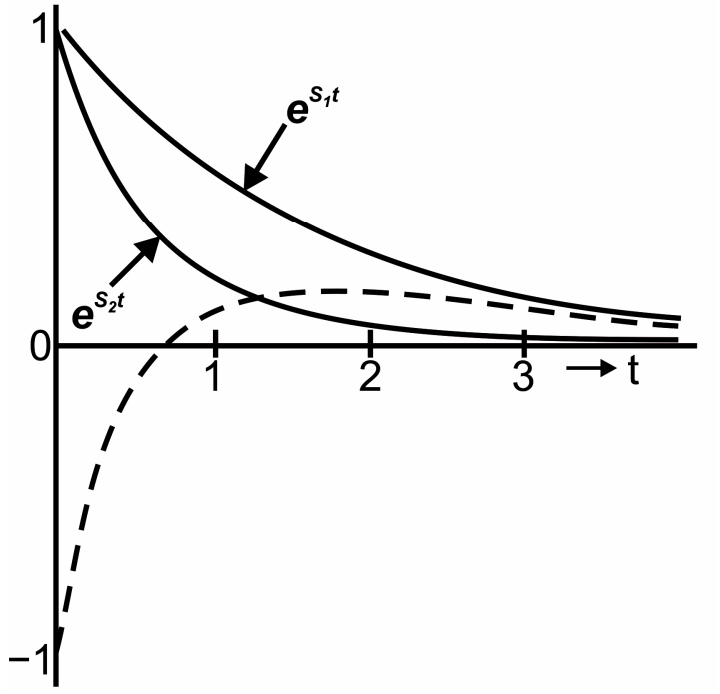


Figure 19. Motions of a highly damped mechanical system.

Without delving into specific cases or calculating the values of C_1 and C_2, the figure illustrates that the motion does not exhibit 'vibration', but rather a gradual return to the

equilibrium position. As observed by comparing Figures 18 and 19, certain similarities between the displayed diagrams are evident. This observation led to the idea of determining the cutting process damping coefficient based on the experimental results and the modal parameters of the machining system, applying methodologies for evaluating stiffness in highly damped systems.

Equating Equations (8) and (13) and implementing their solution into the algorithm for the Fourier series method, the stability lobe diagram definition developed a stability diagram that takes process damping into account (Figure 20). It was assumed that the process damping coefficient is considered only for spindle speeds below 4000 rpm. This limitation was established based on the results of previously conducted experimental investigations.

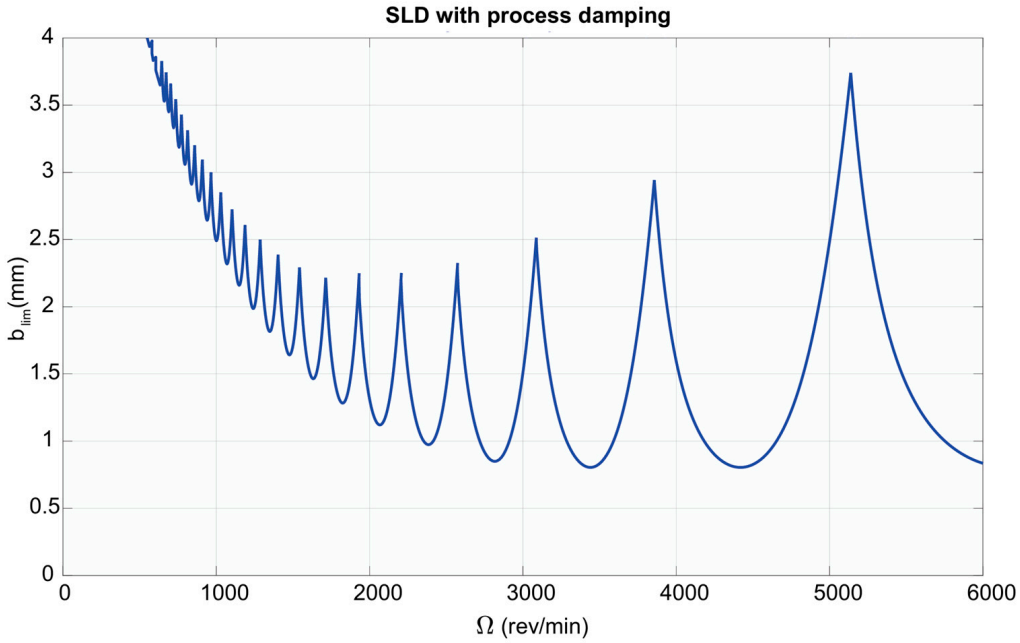


Figure 20. The SLD with process damping for EMCO ConceptMill 450 machining center created by an improved Fourier series method.

By implementing the experimentally determined process damping coefficient into the algorithm for defining the stability lobe diagram (SLD), and by inputting identical initial data as used in the definition of the SLD shown in Figure 13, an SLD that accounts for process damping in the specific machining system was defined.

5. Verification of the Predicted Stability Lobe Diagram with Process Damping

The verification of the proposed methodology for determining the process damping coefficient and its implementation in the model for defining the SLD is conducted to validate its accuracy and applicability. This verification process is particularly challenging because any modification to the machining system alters its modal parameters, directly impacting the defined SLD's reliability and accuracy. However, since the frequency of self-excited vibrations and the cutting tool geometry have the greatest impact on the process damping coefficient, an experimental test was designed to verify the proposed method. In this test, the modal parameters of the machining system were varied, while the cutting tool geometry remained constant.

The machining system modal parameters were determined through experimental modal analysis, as shown in Table 5. It is also worth noting that the variation in modal

parameters was achieved by using two different tool holders with effective lengths of 80 mm and 120 mm (Figure 21).

Table 5. Parameters needed to define the SLD.

Effective length of tool holder:	80 mm	120 mm
Natural frequency in the X-axis direction:	$\omega_{nx} = 1132$ Hz	$\omega_{nx} = 1238$ Hz
Damping coefficient in the X-axis direction:	$\zeta_x = 0.02$	$\zeta_x = 0.03$
Modal stiffness in the X-axis direction:	$k_x = 9.1{\cdot}10^7$ N/m	$k_x = 7.04{\cdot}10^8$ N/m
Natural frequency in the Y-axis direction:	$\omega_{ny} = 1118$ Hz	$\omega_{ny} = 1220$ Hz
Damping coefficient in the Y-axis direction:	$\zeta_y = 0.034$	$\zeta_y = 0.031$
Modal stiffness in the Y-axis direction:	$k_y = 5.32{\cdot}10^7$ N/m	$k_y = 3.07{\cdot}10^7$ N/m
Tool entry angle:	$\phi_{st} = 0^\circ$	
Tool exit angle:	$\phi_{ex} = 180^\circ$	
Cutting tool characteristics (diameter and number of teeth):	$d = 10$ mm; $N_t = 4$	

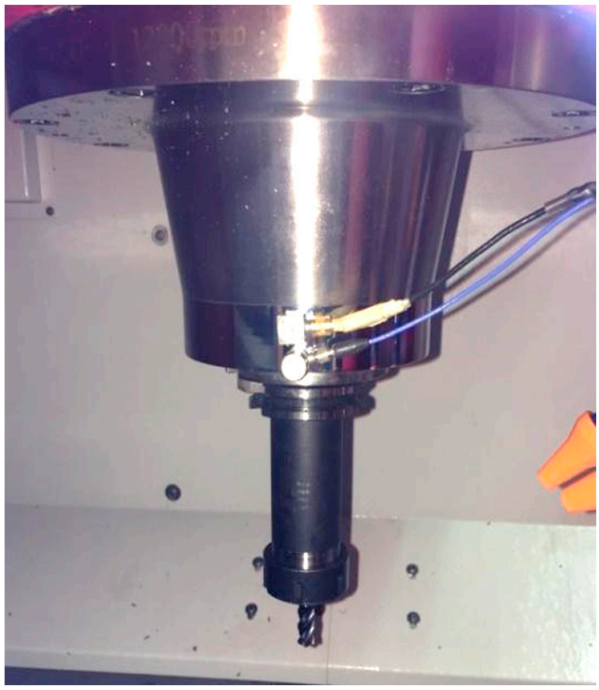


Figure 21. Tool holder with an effective length of 120 mm.

Based on the parameters in the previous table, two stability lobe diagrams (SLDs) were generated using the improved Fourier series method corresponding to tool holders of different lengths. Figure 22 illustrates the SLD with process damping for a tool holder with an effective length of 80 mm, while Figure 23 depicts the SLD for a tool holder with an effective length of 120 mm.

To validate the previously defined stability lobe diagrams, experimental tests were conducted. The machining process of a 42CrMo4 steel workpiece was replicated on the EMCO ConceptMill 450 machining center utilizing a 10 mm diameter high-speed steel tool with a titanium–aluminum–nitride (TiAlN) coating. The feed rate was kept constant at 0.02 mm/tooth, and suitable tool holders were utilized. For both tool holders, three experiments were carried out at spindle speeds of 1000, 1500, and 2000 rpm, while the depth of cut was incrementally increased by 0.4 mm from an initial value of 0.4 mm with

each tool pass. While a 0.4 mm increment may seem coarse, previous research by the authors shows that smaller increments do not notably improve the accuracy of determining the limit cutting depths, but significantly prolong the experiments. The test procedure was identical to that used in the experimental determination of the cutting process damping and will not be explained again, and the occurrence of self-excited vibrations was detected once again by applying frequency analysis to the vibration signal for each tool pass.

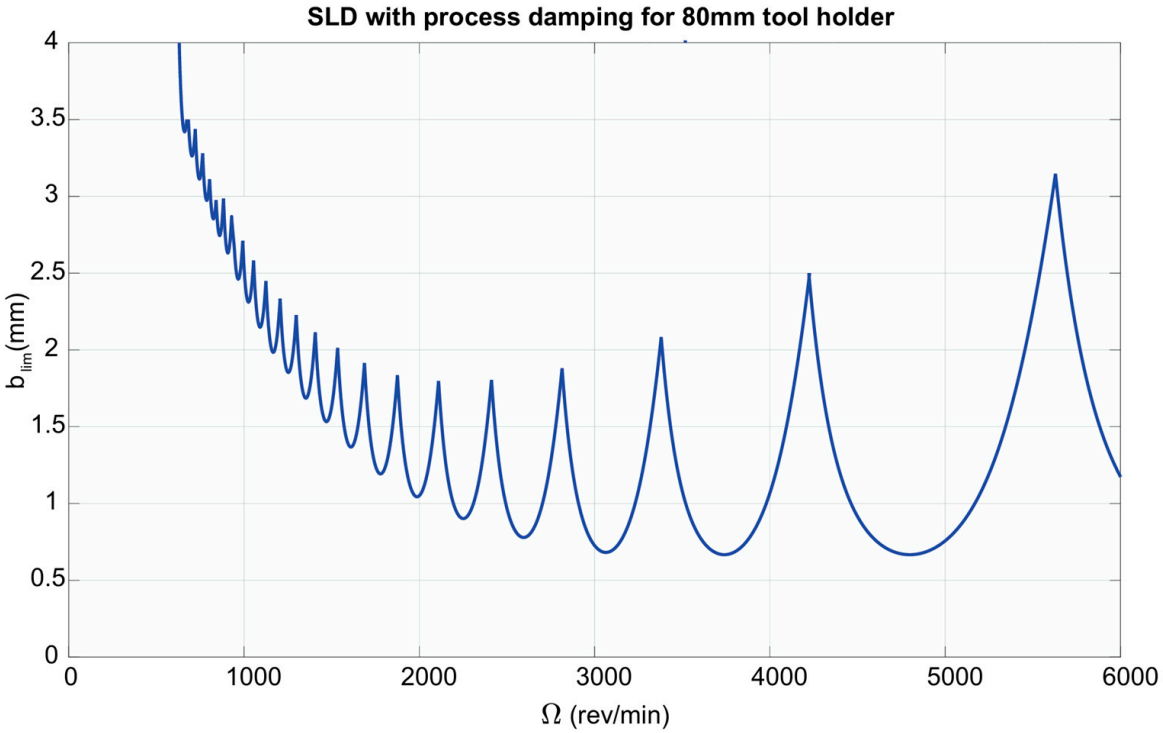


Figure 22. SLD including process damping for an 80 mm tool holder.

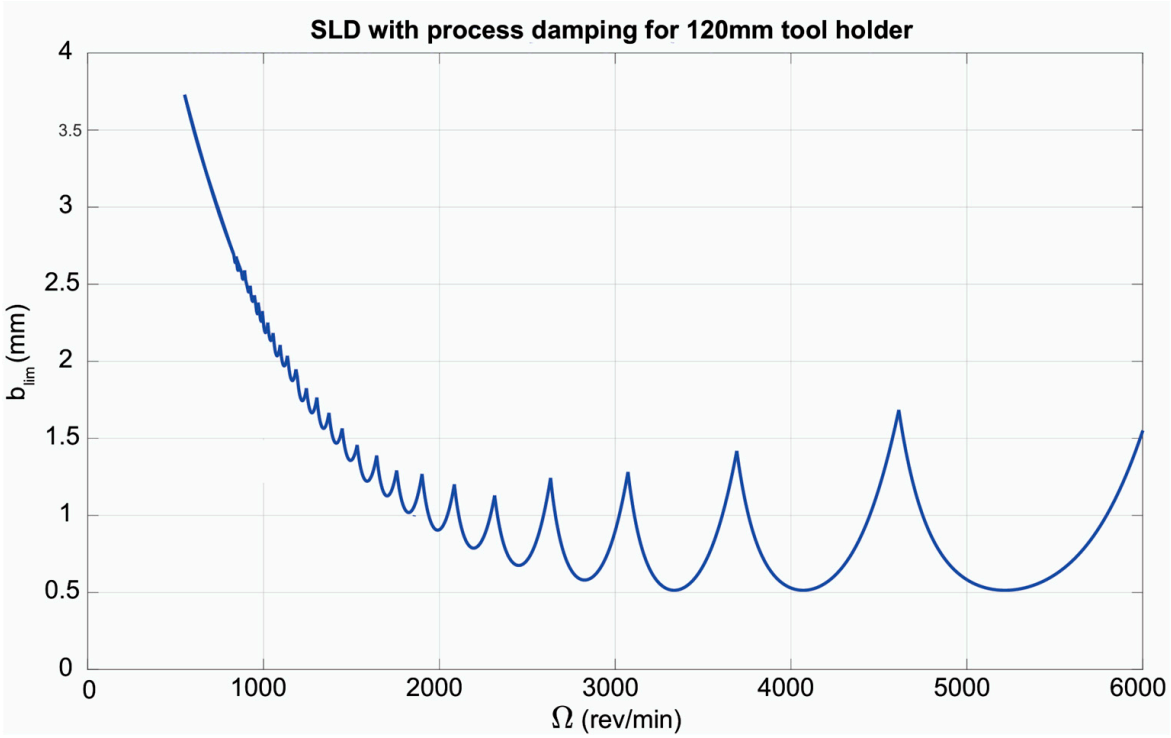


Figure 23. SLD including process damping for a 120 mm tool holder.

The results of these experimental examinations are presented in Figure 24 and Table 6 for the 80 mm tool holder and Figure 25 and Table 7 for the 120 mm tool holder.

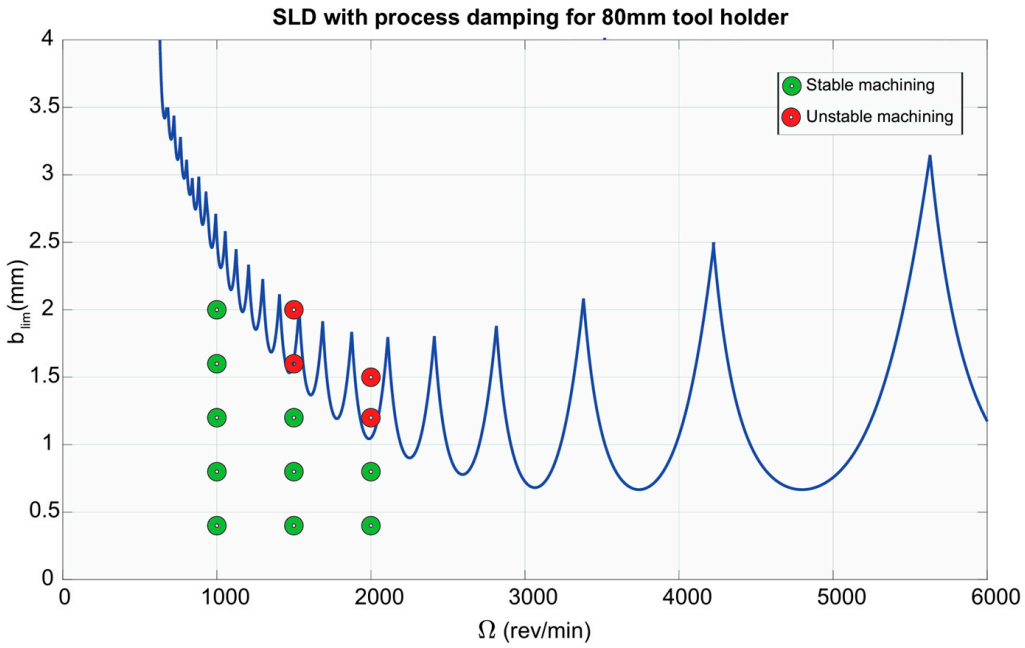


Figure 24. Verification of the defined SLD with process damping for an 80 mm tool holder.

Table 6. Limiting depths of cut defined by experimental tests and from SLD with process damping for an 80 mm tool holder.

No.	Spindle Speed (rev/min)	b_{lim} (mm)		Deviation (%)
		Experiment	Improved SLD	
1.	1000	2.2	2.3	−4.5
2.	1500	1.6	1.58	1.25
3.	3200	1.2	1.15	4

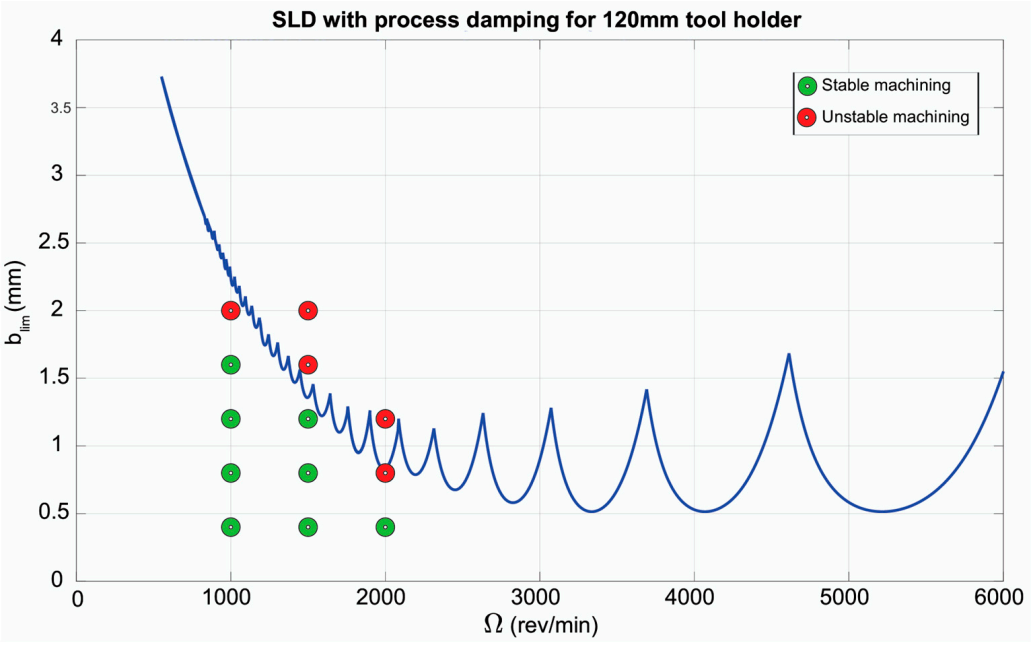


Figure 25. Verification of the defined SLD with process damping for a 120 mm tool holder.

Table 7. Limiting depths of cut defined by experimental tests and from SLD with process damping for a 120 mm tool holder.

No.	Spindle Speed (rev/min)	b_{lim} (mm)		Deviation (%)
		Experiment	Improved SLD	
1.	1000	2	2.16	−8
2.	1500	1.6	1.45	9.3
3.	3200	0.8	0.81	−1.25

6. Discussion

The findings of this study address a critical limitation in the widely used Fourier series method for defining stability lobe diagrams (SLDs) in machining [24–26].

Initial tests highlighted the method's inability to accurately predict machining stability at lower spindle speeds, primarily due to the omission of process damping effects. This gap was addressed by experimentally determining the process damping coefficient and incorporating it into an improved algorithm for SLD generation.

The experimental verification of the proposed methodology for determining the process damping coefficient, conducted with two tool holders of varying lengths, demonstrated the robustness of the improved Fourier series method. By maintaining constant cutting geometry, the influence of tool holder length on the machining system's modal parameters was isolated, providing a focused assessment of the algorithm's performance. The results presented in Figures 24 and 25 confirm the accuracy of the stability predictions, even at lower spindle speeds. These findings suggest that the improved algorithm effectively resolves the shortcomings of the original Fourier series method in low-speed machining scenarios.

Moreover, this study emphasizes the importance of considering process damping as a dynamic factor in stability modeling. The consistency between the experimental results and the predicted stability lobe diagrams underscores the practicality of the improved method for industrial applications in accordance with the findings in studies [27–30]. However, the studies were limited to specific cutting conditions and tool geometries. Additional investigations are required to generalize the methodology to broader machining scenarios, including varying tool geometries and materials.

7. Conclusions

This study successfully demonstrated the enhancement of the Fourier series method for defining stability lobe diagrams (SLDs) by incorporating the process damping coefficient. The improved algorithm significantly increased the accuracy of stability predictions at lower spindle speeds, addressing a critical limitation of the original method.

Experimental validation included tests with tool holders of 80 mm and 120 mm in length, which influenced the machining system's modal parameters. For the 80 mm tool holder, the maximum deviation between the experimentally determined and predicted critical cutting depths was 4.5% (Table 6). For the 120 mm tool holder, the maximum deviation was higher at 9.3% (Table 7). However, this larger deviation is attributed to the experimental depth of cut increment of 0.4 mm, which could be reduced in future tests to achieve greater accuracy in experimental data and further minimize the deviation.

In contrast, the classical Fourier series method, which does not account for process damping, exhibited deviations of up to 52%. This comparison highlights the significant improvement achieved by incorporating process damping into the algorithm. The enhanced method effectively reduces prediction errors to less than 10%, even for cases with varying modal parameters of the machining system.

This study confirms that process damping plays a stabilizing role in machining, particularly at lower spindle speeds. By accurately accounting for this phenomenon, the improved algorithm provides more reliable stability predictions, enabling the better planning and execution of machining operations.

Future research should focus on analyzing the influence of cutting tool geometry on process damping and refining experimental procedures to enhance the accuracy of limit cutting depth definition. Expanding the methodology to include different materials and machining conditions will further increase its industrial applicability.

Additionally, the presented work provides a solid foundation for future studies aimed at developing a comprehensive mathematical description of the process damping coefficient, eliminating the need for experimental testing.

Author Contributions: Conceptualization, C.M. and A.Z.; methodology, C.M. and M.K.; software, V.I. and D.M.; validation, K.M.; investigation, C.M.; resources, K.M. and A.Z.; writing—original draft preparation, C.M.; writing—review and editing, K.M. and C.M.; visualization, M.K. and D.M.; supervision, K.M.; project administration, K.M.; funding acquisition, K.M. All authors have read and agreed to the published version of the manuscript.

Funding: The article was prepared thanks to the support of the Ministry of Education, Science, Research and Sport of Slovak Republic through the grant KEGA 042TUKE-4/2025.

Data Availability Statement: The data that support the findings of this study are available from the corresponding author upon reasonable request.

Acknowledgments: The paper presents a part of the research results of the project "Management of machining process parameters using artificial intelligence tools in production" No. 000827481 2024 09418 003 000 000 001 01 001, supported by the Provincial Secretariat for Higher Education and Scientific Research of the Autonomous Province of Vojvodina. The authors would also like to express their gratitude to the Ministry of Education, Science, Research and Sport of Slovak Republic for the support of the research through the grant KEGA 042TUKE-4/2025.

Conflicts of Interest: The authors declare no conflicts of interest.

References

1. Quintana, G.; Ciurana, J. Chatter in Machining Processes: A Review. *Int. J. Mach. Tools Manuf.* **2011**, *51*, 363–376. [CrossRef]
2. Altintaş, Y.; Budak, E. Analytical Prediction of Stability Lobes in Milling. *CIRP Ann.* **1995**, *44*, 357–362. [CrossRef]
3. Tlustý, J.; Polacek, M. *The Stability of the Machine TooI Against Self-Excited Vibration in Machining*; ASME: New York, NY, USA, 2007.
4. Mladjenovic, C. Dynamic Behavior of Micromachining Systems. Doctoral Thesis, University of Novi Sad, Novi Sad, Serbia, 2020.
5. Budak, E.; Tunc, L.T. Identification and Modeling of Process Damping in Turning and Milling Using a New Approach. *CIRP Ann.* **2010**, *59*, 403–408. [CrossRef]
6. Altintas, Y.; Eynian, M.; Onozuka, H. Identification of Dynamic Cutting Force Coefficients and Chatter Stability with Process Damping. *CIRP Ann.* **2008**, *57*, 371–374. [CrossRef]
7. Eynian, M. Chatter Stability of Turning and Milling with Process Damping. Doctoral Thesis, The University of British Columbia, Vancouver, Canada, 2010.
8. Gurdal, O.; Ozturk, E.; Sims, N.D. Analysis of Process Damping in Milling. *Procedia CIRP* **2016**, *55*, 152–157. [CrossRef]
9. Turkes, E.; Orak, S.; Neseli, S.; Yaldiz, S. A New Process Damping Model for Chatter Vibration. *Measurement* **2011**, *44*, 1342–1348. [CrossRef]
10. Tyler, C.T.; Schmitz, T.L. Analytical Process Damping Stability Prediction. *J. Manuf. Process.* **2013**, *15*, 69–76. [CrossRef]
11. Tyler, C.T.; Troutman, J.; Schmitz, T.L. Radial Depth of Cut Stability Lobe Diagrams with Process Damping Effects. *Precis. Eng.* **2015**, *40*, 318–324. [CrossRef]
12. Wan, M.; Feng, J.; Ma, Y.; Zhang, W. Identification of Milling Process Damping Using Operational Modal Analysis. *Int. J. Mach. Tools Manuf.* **2017**, *122*, 120–131. [CrossRef]
13. Orak, S.; Turkes, E.; Selvi, S.; Karabeyoglu, S.S. Process Damping Model Approach in Milling Operations. *J Braz. Soc. Mech. Sci. Eng.* **2021**, *43*, 519. [CrossRef]
14. Feng, J.; Liu, X.-T. Mechanism and Modeling of Machining Process Damping: A Review. *Int. J. Adv. Manuf. Technol.* **2023**, *127*, 1045–1069. [CrossRef]

15. Kurata, Y.; Merdol, S.D.; Altintas, Y.; Suzuki, N.; Shamoto, E. Chatter Stability in Turning and Milling with in Process Identified Process Damping. *J. Adv. Mech. Des. Syst. Manuf.* **2010**, *4*, 1107–1118. [CrossRef]
16. Li, X.; Zhao, W.; Li, L.; He, N.; Chi, S. Modeling and Application of Process Damping in Milling of Thin-Walled Workpiece Made of Titanium Alloy. *Shock Vib.* **2015**, *2015*, 431476. [CrossRef]
17. Taylor, C.M.; Sims, N.D.; Turner, S. Process Damping and Cutting Tool Geometry in Machining. *IOP Conf. Ser. Mater. Sci. Eng.* **2011**, *26*, 012009. [CrossRef]
18. Yusoff, A.R.; Turner, S.; Taylor, C.M.; Sims, N.D. The Role of Tool Geometry in Process Damped Milling. *Int. J. Adv. Manuf. Technol.* **2010**, *50*, 883–895. [CrossRef]
19. Tyler, C.T.; Schmitz, T.L. Process Damping Milling Model Database. *Proc. NAMRI/SME* **2014**, *42*, 325–334.
20. Tang, A.J.; Liu, Z.Q. Effect of Helix Angle and Normal Rake Angle on Stability in End Milling. *Adv. Mater. Res.* **2009**, *69–70*, 394–398. [CrossRef]
21. Schmitz, T.L.; Smith, K.S. *Machining Dynamics: Frequency Response to Improved Productivity*; Springer International Publishing: Cham, Switzerland, 2019; ISBN 978-3-319-93706-9.
22. Kalajdzic, M. *Cutting Technology: Manual*; Faculty of Mechanical Engineering, University of Belgrade: Belgrade, Serbia, 2004; ISBN 86-7083-345-X.
23. Hartog, J.P.D. *Mechanical Vibrations*; Dover Publications: Mineola, NY, USA, 2013; ISBN 978-0-486-13185-6.
24. Kosarac, A.; Cep, R.; Trochta, M.; Knezev, M.; Zivkovic, A.; Mladjenovic, C.; Antic, A. Thermal Behavior Modeling Based on BP Neural Network in Keras Framework for Motorized Machine Tool Spindles. *Materials* **2022**, *15*, 7782. [CrossRef]
25. Kosarac, A.; Mladjenovic, C.; Zeljkovic, M.; Tabakovic, S.; Knezev, M. Neural-Network-Based Approaches for Optimization of Machining Parameters Using Small Dataset. *Materials* **2022**, *15*, 700. [CrossRef] [PubMed]
26. Živković, A.M.; Zeljković, M.V.; Mladjenovic, C.D.; Tabaković, S.T.; Milojević, Z.L.; Hadžistević, M.J. A Study of Thermal Behavior of the Machine Tool Spindle. *Therm. Sci.* **2019**, *23*, 2117–2130. [CrossRef]
27. Karmiris-Obratanski, P.; Thangaraj, M.; Leszczyńska-Madej, B.; Markopoulos, A.P. Advanced Machining Technology for Modern Engineering Materials. *Materials* **2024**, *17*, 2064. [CrossRef]
28. Monka, P.P.; Monkova, K.; Majstorovic, V.D.; Božić, Ž.; Andrej, A. Optimal Cutting Parameter Specification of Newly Designed Milling Tools Based on the Frequency Monitoring. *Int. J. Adv. Manuf. Technol.* **2021**, *115*, 777–794. [CrossRef]
29. Sahraoui, Z.; Mehdi, K.; Jaber, M.B. Experimental Study of the Dynamic Behavior of Thin-Walled Tubular Workpieces in Turning Cutting Process. *J. Adv. Manuf. Syst.* **2021**, *20*, 75–93. [CrossRef]
30. Dombovari, Z.; Stepan, G. The Effect of Helix Angle Variation on Milling Stability. *J. Manuf. Sci. Eng.* **2012**, *134*, 051015. [CrossRef]

Disclaimer/Publisher's Note: The statements, opinions and data contained in all publications are solely those of the individual author(s) and contributor(s) and not of MDPI and/or the editor(s). MDPI and/or the editor(s) disclaim responsibility for any injury to people or property resulting from any ideas, methods, instructions or products referred to in the content.